Hazy Image Restoration by Bi-Histogram Modification

BO-HAO CHEN, SHIH-CHIA HUANG, and JIAN HUI YE,
National Taipei University of Technology

Visibility restoration techniques are widely used for information recovery of hazy images in many computer vision applications. Estimation of haze density is an essential task of visibility restoration techniques. However, conventional visibility restoration techniques often suffer from either the generation of serious artifacts or the loss of object information in the restored images due to uneven haze density, which usually means that the images contain heavy haze formation within their background regions and little haze formation within their foreground regions. This frequently occurs when the images feature real-world scenes with a deep depth of field. How to effectively and accurately estimate the haze density in the transmission map for these images is the most challenging aspect of the traditional state-of-the-art techniques. In response to this problem, this work proposes a novel visibility restoration approach that is based on Bi-Histogram modification, and which integrates a haze density estimation module and a haze formation removal module for effective and accurate estimation of haze density in the transmission map. As our experimental results demonstrate, the proposed approach achieves superior visibility restoration efficacy in comparison with the other state-of-the-art approaches based on both qualitative and quantitative evaluations. The proposed approach proves effective and accurate in terms of both background and foreground restoration of various hazy scenarios.

Categories and Subject Descriptors: I.4.5 [**Image Processing and Computer Vision**]: Reconstruction—*Transform methods*

General Terms: Design, Algorithms

Additional Key Words and Phrases: Visibility restoration, transmission map, haze density

ACM Reference Format:
Bo-Hao Chen, Shih-Chia Huang, and Jian Hui Ye. 2015. Hazy image restoration by Bi-Histogram modification. ACM Trans. Intell. Syst. Technol. 6, 4, Article 50 (July 2015), 17 pages.
DOI: http://dx.doi.org/10.1145/2710024

1. INTRODUCTION

Restoration of visibility in outdoor images is the first essential step of information recovery in many computer vision systems, including traffic status detection [Song et al. 2013], vehicular traffic tracking [Zhang et al. 2012], video surveillance [Huang and Chen 2014], traffic sign recognition, and so on [Li et al. 2013; Ma et al. 2012].

In such applications, robust recognition and extraction of objects in inclement weather calls for an effective and reliable visibility restoration approach that could be characterized by its ability to estimate unknown haze density. These approaches can be divided into the following categories: non-single-image processing [Kopf et al.

This work was supported by the Ministry of Science and Technology of the Republic of China under Grant Nos. MOST 103-2221-E-027-030-MY2 and MOST 103-2221-E-027-031-MY2.
Authors' addresses: B.-H. Chen, S.-C. Huang (corresponding author), and J. H. Ye, Department of Electronic Engineering, National Taipei University of Technology, Taipei 106, Taiwan; emails: {bhchen, schuang, t102419017}@ntut.edu.tw.

DOI: http://dx.doi.org/10.1145/2710024

2008; Narasimhan and Nayar 2003a, 2003b; Nayar and Narasimhan 1999; Schechner et al. 2003; Tan and Oakley 2000], which uses either geometrical information or multiple images of the same scene; and single-image processing [Fattal 2008; He et al. 2011; Nishino et al. 2012; Tan 2008; Tarel and Hautiere 2009; Xie et al. 2010; Xu et al. 2012; Yeh et al. 2013], which takes advantage of strong priors or assumptions via only a single hazy image. In the absence of geometry information and multiple images, the most widely adopted approach for visibility restoration in hazy scenes is based on single-image processing.

To obtain the haze density from a hazy image, the approach of Tan [2008]—which is based on an observation that the contrast ratio of the haze-free images is evidently higher than in the hazy images—is applied to achieve visibility restoration by maximizing the local contrast. However, the restored image usually suffers from serious artifact generation along depth edges since the use of Tan's approach readily overcompensates for reduced contrast. Fattal [2008] applied an assumption that scene transmission and the shading are locally uncorrelated and estimated the scene transmission based on independent component analysis in order to remove haze formation from hazy images. Nevertheless, the use of Fattal's approach is not reliable when images suffer from significant haze formation; as such, they may be locally recovered.

Moreover, Tarel and Hautiere [2009] proposed an approach for estimating the atmospheric veil from hazy images based on the conjunctive utilization of the minimum, maximum, and median filters. The image can subsequently be restored by using the atmospheric veil. Unfortunately, this method is sensitive to scene depth discontinuities, and readily results in halo artifacts and color tone changes in the restored image. This is due to the fact that their restoration effectiveness depends greatly on the appropriate filter operations. Nishino et al. [2012] proposed a Bayesian probabilistic method for visibility restoration via a single foggy image, which estimates the scene depth and albedo utilizing a factorial Markov random field. However, the images restored by Nishino et al. usually result in serious artifacts in sky regions due to the fact that this approach only roughly estimates the scene depth and albedo. In addition, Xie et al. [2010] employed the image fusion strategy to seamlessly blend several scales of luminance map via the multi-scale Retinex algorithm in which a pseudo scene depth can be produced. However, the use of simulated scene depth for haze removal usually results in excessive restoration of the foreground regions of the restored image.

He et al. [2011] built their approach on a key observation that the color channels of a haze-free outdoor image within the local patch contain at least one channel belonging to a very low-intensity value. According to this observation, the dark channel prior method has been proposed to remove haze formation from hazy images in which haze thickness can be estimated as a transmission map by using a combination of two minimum operators. Of the various single-image processing strategies, this is the most widely used approach for visibility restoration of images of outdoor scenes [Chiang and Chen 2012; Shiau et al. 2013]. Additionally, several methods [Xu et al. 2012; Yeh et al. 2013] based on the dark channel prior have been popularly developed and implemented by many visibility restoration applications.

Xu et al. [2012] proposed an improved method by employing the bilateral filter to refine the transmission map, after which the restored image can be produced through application of a constant factor as the main criterion for enhancing the adaptability of visibility restoration. In addition, Yeh et al. developed a dehazing framework in Yeh et al. [2013] that removes haze formation from hazy images by producing an improved transmission map from the conjunctive utilization of the pixel-based dark channel prior and the pixel-based bright channel prior.

In general, the use of the dark channel prior based technique via the methods of He et al., Xu et al., and Yeh et al. can produce passable restoration results in images

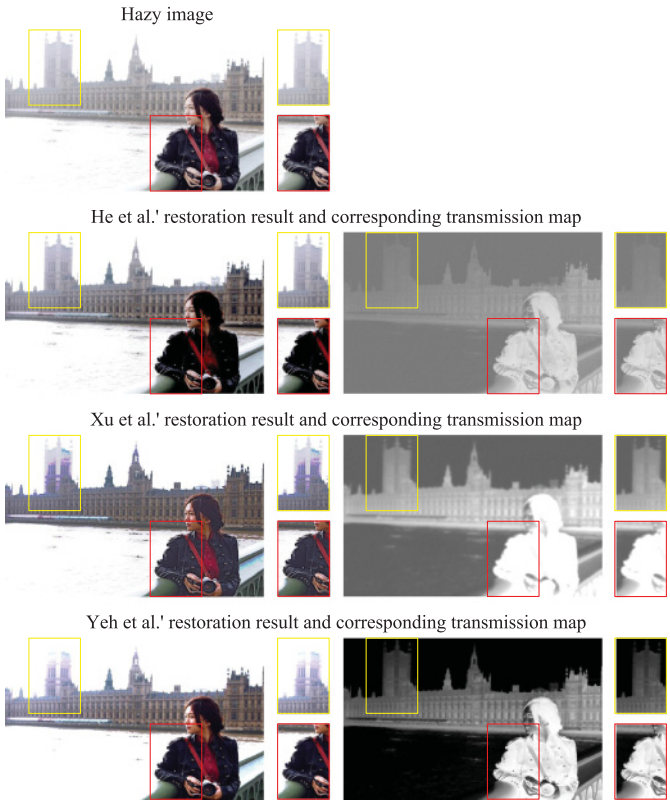

Fig. 1. Performance comparison of the haze removal methods of He et al., Xu et al., and Yeh et al. in regard to hazy images in which only the background areas contain haze formation.

with uniform haze, as indicated in He et al. [2011], Xu et al. [2012], and Yeh et al. [2013]. In such an ideal images, the haze density is easily estimated by using the dark channel prior in the transmission map. However, the use of these dark channel prior based techniques often results in inaccurate estimation of haze density when the captured images contain haze only in their background areas, thereby producing an unbalanced transmission map. This typically occurs in images of real-world scenes with deep depths of field. Hence, effective visibility restoration for computer vision systems can be a problem for these methods.

An example shown in Figure 1 demonstrates that the unbalanced transmission map of these methods may not be applicable for recovering visibility in images with haze formation in only their background regions (see the yellow box of Figure 1). In addition, the foreground region (see the red box of Figure 1) contains few haze effects. In this situation, the approach of He et al. not only excessively restores the foreground region of the hazy image, but also inefficiently recovers the background region. This is because the method of He et al. overestimates and underestimates the transmission map of the foreground and background regions, respectively. Although the approaches of Xu et al. and Yeh et al. passably restore foreground regions of hazy image, some relevant background pixels are excessively restored; this results in cavities inside building structures. This is due to overestimation of the haze density of background regions in the transmission maps produced by the methods of Xu et al. and Yeh et al.

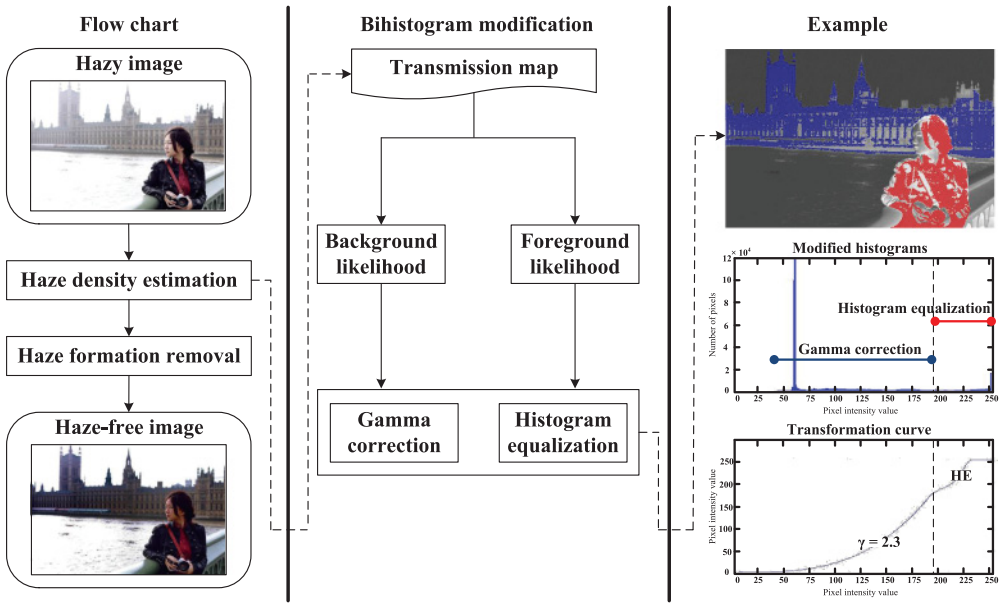

Fig. 2. Architecture of the proposed Bi-Histogram modification-based haze removal method.

In this article, we propose a novel approach based on Bi-Histogram modification that exploits the features of gamma correction and histogram equalization, and combines them in order to flexibly adjust haze thickness in the transmission map. Subsequently, effective and accurate visibility restoration can be achieved. The primary contribution of this article is the integration of two types of histogram modifications in the restoration process to enhance haze removal of background regions and maintain information of the foreground objects. This yields higher quality, haze-free images that are less prone to artifacts in comparison with the other state-of-the-art methods. Experimental results via qualitative and quantitative evaluations of a variety of hazy test images indicate that our Bi-Histogram modification-based visibility restoration approach can effectively remove haze formation and completely recover object structures.

The rest of this article is organized as follows. We describe the proposed Bi-Histogram modification technique in the next section. In Section III, we compare the proposed dehazing method to the other state-of-the-art techniques through qualitative and quantitative evaluations. Finally, the conclusion is presented in Section IV.

2. PROPOSED METHOD

In this section, we describe how the proposed method estimates haze density and removes haze formation from single hazy images of realistic scenes. The main aim of the proposed method is to compensate the unbalanced transmission map by which to recover the visibility of background regions of hazy images with high efficacy, limiting false restorations (excessive restoration of the foreground pixels of an object) as much as possible. To this end, the proposed method consists of two major modules (see Figure 2): a Haze Density Estimation (HDE) module and a Haze Formation Removal (HFR) module.

First of all, the proposed HDE module is designed by the Bi-Histogram modification technique to flexibly adjust either overestimated or underestimated haze thickness in the adjusted transmission map in order to accomplish effective estimation of haze density from the captured hazy image. After haze thickness is accurately estimated by

Table I. Variable Notation used in the Proposed Method

Symbols	Meanings
r, g, b	Red, green, and blue channel values of a pixel in an arbitrary image RGB
x, y	The position of a pixel in an arbitrary image
i, j	The position of a pixel in an arbitrary patch
c	The index of each RGB color channel
A	The global atmospheric light
I	The input hazy image 原图像
J	The output haze-free image 处理后图像
A^c	The c component decomposed from A
I^c	The c component decomposed from I
J^c	The c component decomposed from J
t	The transmission map refined from $\tilde{t}$
I^d	The dark channel of I
Ω	The size for a patch
$\tilde{t}$	The transmission map without refinement processing
ω	The constant factor
t_F	The foreground-likelihood transmission map of t
t_B	The background-likelihood transmission map of t
ρ_m	The average intensity value of ρ
ρ	The set space from t
t_m	The average intensity value of t
$\tilde{t}_F$	The corrected foreground-likelihood transmission map of t_F
$\tilde{t}_B$	The enhanced background-likelihood transmission map of t_B
v	The intensity value within an arbitrary image
$v_{max}^{t_F}$	The maximum value of t_F
C_{t_F}	The cumulative probability density of t_F
$v_{max}^{t_B}$	The maximum value of t_B
γ	The constant factor
E_t	The entropy intensity of t
v_{max}	The maximum value of t
P_t	The probability mass function of t
$\bar{t}$	The transmission map adjusted from t
α	The constant factor

the HDE module, the proposed HFR module is then used to completely remove haze formation and accurately recover the scene radiance of real-world environments during hazy weather conditions. By doing so, we demonstrate that the proposed Bi-Histogram modification-based haze removal method is able to effectively restore visibility in hazy images. The symbols used in the methodology description of the proposed method are summarized in the Table I.

2.1. Haze Density Estimation Module

Atmosphere-turbid mediums, such as hazy particles, irregularly absorb and scatter observed light during poor weather conditions. According to this atmospheric phenomenon, an optical model was proposed to represent the formation of a hazy image [Oakley and Satherley 1998]. Let (r, g, b) represent red, green, and blue channel values of a pixel in an arbitrary image. Thus, the model can be expressed for each pixel as follows:

$$I^c(x, y) = J^c(x, y)\, t(x, y) + A^c(1 - t(x, y)), \tag{1}$$

where $I(x, y)$, $J(x, y)$, and $t(x, y)$ represent the intensity values of the pixels at position (x, y) in the captured hazy image, the ideal haze-free image, and the transmission map, respectively. Moreover, A is the global atmospheric light and c is the index of each RGB color channel.

With this model, the scene depth of hazy image can be derived by using the dark channel prior via the observation that there is at least one very low-intensity value for each channel of a pixel within most of the non-sky patches in an arbitrary haze-free image [He et al. 2011]. In contrast with this property, there are higher intensity values within the regions containing large amounts of haze formation. For each incoming image, the dark channel I^d of a hazy image I can be expressed as follows:

$$I^d(x, y) = (x, y) \in \Omega(i, j) \min\left(c \in \{r, g, b\} \min I^c(x, y)\right), \tag{2}$$

where $J^d(x, y)$ represents the minimum intensity value of the pixels within the corresponding patch Ω of position (i, j) after minimally processing the hazy image I at position (x, y) for each color channel.

Next, the transmission map $\tilde{t}$, which is regarded as haze density, can be produced by using an inversion of the dark channel as follows:

$$\tilde{t}(x, y) = 1 - \omega I^d(x, y), \tag{3}$$

where ω represents a constant factor for preserving distant objects, which can be set to 0.95 according to He et al. [2011]. However, the restored image usually suffers from serious halo effects when using this transmission map. Thus, the soft matting technique [Levin et al. 2008] is used to refine the transmission map in order for the halo effect to be restrained in the restored image.

As was mentioned in the previous section, the production of a transmission map for complete estimation of haze density in images containing haze formation only within the background area is a challenging task for traditional state-of-the-art methods. Accordingly, we first analyze the correlation between the background likelihood and foreground likelihood from the refined transmission map t to compose two set spaces. As such, the haze density of each likelihood can be flexibly adjusted by using the Bi-Histogram modification technique to circumvent this problem. According to the property of transmission map, haze density thickens as distance increases. Based on this characteristic, we can effectively decompose the transmission map into a foreground-likelihood transmission map t_F and a background-likelihood transmission map t_B as follows:

$$t = t_F \cup t_B, \tag{4}$$

where

$$t_F = \{t(x, y) | t(x, y) > \rho_m, \forall t(x, y) \in t\}, \tag{5}$$

and

$$t_B = \{t(x, y) | t(x, y) \leq \rho_m, \forall t(x, y) \in t\}. \tag{6}$$

Note that ρ_m is defined as the average intensity value of the set space ρ. Moreover, the set space ρ can be composed as follows:

$$\rho = \{t(x, y) | t(x, y) > t_m, \forall t(x, y) \in t\}, \tag{7}$$

where t_m represents the average intensity value of the transmission map t.

The foreground haze density likelihood of the refined transmission map t is usually overestimated, as mentioned in the previous section. Consequently, the most frequent intensity values of the foreground-likelihood transmission map should be automatically spread to the highest levels of the histogram for diminishing the haze density. For each incoming pixel of the foreground-likelihood transmission map, the corrected foreground-likelihood transmission map $\bar{t}_F$ can be produced by using histogram equalization as follows:

$$\bar{t}_F(v) = \rho_m + \left(v_{max}^{t_F} - \rho_m\right) C_{t_F}(v), \tag{8}$$

where v represents each intensity value within the foreground-likelihood transmission map t_F. Note that $v_{max}^{t_F}$ and C_{t_F} are the maximum value and the cumulative probability density of the foreground-likelihood transmission map t_F, respectively.

Since the intensities of the background-likelihood transmission map would be distributed between the highest and lowest levels of the histogram through the adjustment of histogram equalization, the background-likelihood transmission map might lose some statistical information for haze density. For this reason, the intensity values of the background-likelihood transmission map should be spread dynamically via the use of self-adaption gamma correction according to the amount of intrinsic information in hazy images. Subsequently, underestimation of haze density in the background-likelihood transmission map can be overcome. Consequently, the higher intensity of the gamma factor generates a more significant adjustment of haze density. For each incoming pixel of the background-likelihood transmission map, the enhanced background-likelihood transmission map $\bar{t}_B$ can be constructed by using the self-adaption gamma correction as follows:

$$\bar{t}_B(v) = v_{max}^{t_B} \left(\frac{t_B(v)}{v_{max}^{t_B}} \right)^{\gamma}, \tag{9}$$

where v represents each intensity value within the background-likelihood transmission map t_B, $v_{max}^{t_B}$ represents the maximum value of the background-likelihood transmission map t_B, and γ represents a constant factor for self-adapting the haze density, which can be expressed as follows:

$$\gamma = \frac{E_t}{2}. \tag{10}$$

Note that E_t is the entropy intensity for the transmission map t as follows:

$$E_t = -\sum_{v=0}^{v_{max}} P_t(v) \log P_t(v), \tag{11}$$

where P_t and v_{max} represent the probability mass function and maximum value of the transmission map t, respectively.

By doing so, the adjusted transmission map $\bar{t}$ with accurate haze density can be expressed as follows:

$$\bar{t} = \bar{t}_F \cup \bar{t}_B, \tag{12}$$

where $\bar{t}_F$ and $\bar{t}_B$ represent the corrected foreground-likelihood transmission map and the enhanced background-likelihood transmission map, respectively. Note that the adjusted transmission map $\bar{t}$ is refined by using the median filter for preserving edge information after the process of the Bi-Histogram modification. As mentioned previously, the flowchart and the pseudocode of the proposed HDE module are given in Figure 2 and Algorithm 1, respectively.

2.2. Haze Formation Removal Module

After the adjusted transmission map is constructed, the proposed HFR module is able to accurately and completely remove haze formation from images captured in hazy conditions. To this end, the adjusted transmission map $\bar{t}$ is incorporated into the following function:

$$J^c(x, y) = \frac{I^c(x, y) - A^c}{max\left(\bar{t}(x, y), \alpha\right)} + A^c, \text{where } c \in \{r, g, b\}, \tag{13}$$

and α is a constant factor for increasing the exposure of the haze-free image J, which can be set to 0.1 according to He et al. [2011]. Note that A^c can be set to the highest

ALGORITHM 1: The Proposed HDE Module

Input: Hazy image I
Output: Adjusted transmission map $\bar{t}$ and dark channel I^d of I
Initialize: $\omega \leftarrow 0.95$
for each pixel (x, y) **do**
  for each pixel (i, j) in each patch Ω **do**
    $I^d \leftarrow \min\{\min\{I^c \mid c \in (r, g, b)\} \mid \in \Omega\}$
  end for
end for
for each pixel (x, y) **do**
  $\tilde{t} = 1 - \omega I^d$
end for
Refine $\tilde{t}$ *using soft matting procedure on* t
Calculate the mean intensity value t_m *of* t
for each pixel (x, y) **do**
  if $t > t_m$ **then**
    $\rho \leftarrow t$
  end if
end for
Calculate the mean intensity value ρ_m *of* ρ
for each pixel (x, y) **do**
  if $t > \rho_m$ **then**
    $t_F \leftarrow t$
  else
    $t_B \leftarrow t$
  end if
end for
Calculate the cumulative distribution functions C_{t_F} of t_F
Calculate the probability mass function P_t of t
for each intensity value $v \in \mathbb{N}^0 \wedge v \leq v_{max}$ **do**
  $E_t \leftarrow -\sum P_t(v) \log P_t(v)$
end for
$\gamma \leftarrow E_t / 2$
$v_{max}^{t_F} \leftarrow \max\{t(x, y) \in t_F\}$
$v_{max}^{t_B} \leftarrow \max\{t(x, y) \in t_B\}$
for each intensity value $v \in \mathbb{N}^0 \wedge v \leq v_{max}$ **do**
  if $v > \rho_m$ **then**
    $\bar{t}_F(v) \leftarrow \rho_m + (v_{max}^{t_F} - \rho_m) C_{t_F}(v)$
  else
    $\bar{t}_B(v) \leftarrow v_{max}^{t_B} (t_B(v) / v_{max}^{t_B})^{\gamma}$
  end if
end for
$\bar{t} \leftarrow \bar{t}_F \cup \bar{t}_B$
Refine $\bar{t}$ *using median filter on* $\bar{t}$

intensity values for each color channel within the region, which consists of the brightest 0.1% of the dark channel of the input hazy image [He et al. 2011]. In addition, the pseudocode of the proposed HFR module is shown in Algorithm 2 in which the restoration equation (13) and the acquirement of atmospheric light A are explained in detail.

Finally, a high-quality haze-free image can be achieved by using these two proposed modules. As mentioned previously, the framework of the proposed method is shown in Figure 2, which includes two processing modules: the HDE module and the HFR module.

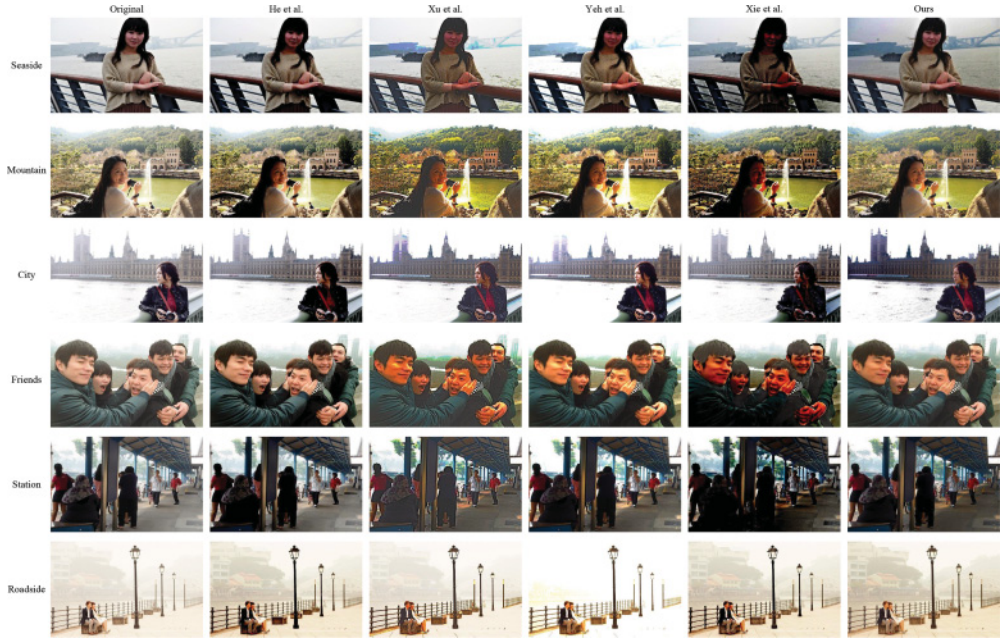

Fig. 3. Performance comparison of the visibility restoration of each method for images with haze formation.

ALGORITHM 2: The Proposed HFR Module

Input: Hazy image I, adjusted transmission map $\bar{t}$, and dark channel I^d of I
Output: Haze-free image J
Initialize: $A^c \leftarrow 0$ and $\alpha \leftarrow 0.1$
for each pixel (x, y) in the brightest 0.1% of I^d **do**
  if $I^c > A^c$ **then**
    $A^c \leftarrow I^c$
  end if
end for
for each pixel (x, y) **do**
  $J^c \leftarrow (I^c - A^c)/\max\{\bar{t}, \alpha\} + A^c$
end for

3. EXPERIMENTAL RESULTS

In the following section, the efficacy of the proposed method is evaluated and compared to the four other state-of-the-art techniques via qualitative and quantitative evaluations. These compared techniques include the methods of He et al. [2011], Xu et al. [2012], Yeh et al. [2013], and Xie et al. [2010], which are discussed in the previous section. To this end, six images captured in realistic scenes during hazy weather conditions were used for testing, named Seaside, Mountain, City, Friends, Station, and Roadside.

3.1. Qualitative Comparison

First, this section conducts a visual assessment of the restored haze-free images. Figure 3 shows six examples that demonstrate the respective performances of the proposed approach and the other compared approaches for six test images captured during hazy weather conditions.

As can be observed in Figure 3, the use of the method of He et al. results in not only insufficient removal of haze formation within the background region, but also inaccurate recovery of the foreground region. This is because the method of He et al. employs the soft matting technique to consistently refine the transmission map in which the haze densities of the background and foreground regions of the transmission map are underestimated and overestimated, respectively. Moreover, the method of Xu et al. uses the constant factor as the main criterion by which to enhance adaptability for hazy scenes when restoring hazy images. Yeh et al. integrate the pixel-based dark channel prior with the bright channel prior to produce a transmission map for haze removal. Although the restored images show improvements over these two methods in regard to recovery of the foreground region, restorations of the background region inevitably suffer from serious holes inside background structures. In addition, the use of the method by Xie et al., which is based on an image fusion strategy, results in underexposure effects of foreground objects since the weight maps produced by using the multi-scale Retinex algorithm are disproportionately blended into the transmission map.

In contrast to these traditional methods, the proposed method is able to produce restored images with more satisfactory foreground and background regions. This is due to the ability of the proposed HDE module to distinguish the foreground likelihood and background likelihood of the transmission map, whereupon the haze density is flexibly adjusted by using the Bi-Histogram modification technique for each region. Consequently, superior restoration results can be achieved by the proposed method, the performance of which demonstrates the efficacy and accuracy of this novel approach.

3.2. Quantitative Comparison

Next, we present the respective efficacies of the compared methods as determined via quantitative evaluation of test hazy images. Since there is no validated reference image for captured realistic scene, quantization of restored haze-free images is a challenging task. In general, quantitative metrics are divided into two major groups: non-reference methods and reference methods.

In order to demonstrate that the proposed method can achieve more complete and accurate visibility restoration in both background and foreground regions of hazy images than can the other state-of-the-art methods, each image is first split into two subimages for quantitative evaluation, including a background image and a foreground image.

Then, e and E metrics, which belong to the non-reference methods, were used to measure the restoration rates of each method in regard to the background images, which contain heavy haze densities [Hautière et al. 2011; Huang et al. 2013]. Specifically, the e metric measures the amount of edge restoration between the restored background image and the original background image with haze formation. The E metric measures the entropy of the image and assesses the content of the background image after and before restoration. They can be calculated as

$$e = \frac{n_r - n_o}{n_o}, \tag{14}$$

$$E = -\sum_{l=0}^{l_{max}} P(l) \log P(l), \tag{15}$$

where n_r and n_0 indicate the total number of visible edges in the restored background image and the original background image, respectively. l indicates each intensity value within the background image, l_{max} indicates the maximum value of the image, and P indicates the probability mass function of the image. Note that the higher values attained via these two metrics signify superior restoration efficacy.

In addition to non-reference methods, the foreground images, which contain few haze effects, were measured by using the reference methods to demonstrate the maintenance of object structures for the original image, including the MD metric and the PSNR metric [Caraffa and Tarel 2013; Huang et al. 2013]. For each restored foreground image and original foreground image, the MD metric and the PSNR metric can be calculated as follows:

$$\mathrm{MD} = \max\left(\mathrm{MSE}^c\right) \pm \epsilon, \tag{16}$$

$$\mathrm{PSNR} = 20\log\left(\frac{l_{max}}{\sqrt{\max\left(\mathrm{MSE}^c\right)}}\right), \tag{17}$$

where

$$\mathrm{MSE}^c = \frac{\sum_{x=1}^{m}\sum_{y=1}^{n}\left(J_f^c(x,y) - I^c(x,y)\right)^2}{mn}, \tag{18}$$

$$\epsilon_{positive} = \frac{\max\left(\mathrm{MSE}^c\right) + \min\left(\mathrm{MSE}^c\right)}{2} - \max\left(\mathrm{MSE}^c\right), \tag{19}$$

and

$$\epsilon_{negative} = \frac{\max\left(\mathrm{MSE}^c\right) + \min\left(\mathrm{MSE}^c\right)}{2} - \min\left(\mathrm{MSE}^c\right). \tag{20}$$

Note that $c \in \{r, g, b\}$ and higher values attained via the PSNR metric indicate superior maintenance efficacy. On the contrary, higher values attained by using the MD metric indicate more serious degradation of foreground objects.

As can be observed in the background images of Figures 4–9, the uses of the methods of He et al. and Xie et al. are obviously incapable of removing haze formation and recovering the edge information from hazy images. Moreover, the methods of Xu et al. and Yeh et al. excessively restore background images and thereby result in either the generation of serious artifacts or the loss of object information. For these reasons, the values attained via e and E metrics are substantially lower for the restoration results produced by the other compared methods than for the results produced by the proposed method.

In addition, the methods of He et al. and Xu et al. employ soft matting and the constant factor to consistently refine the transmission map and inflexibly restore hazy images, respectively. As a result, they fail to retain the intrinsic objects in the foreground images. In addition, the methods of Yeh et al. and Xie et al. are unable to accurately estimate foreground haze density by fusing several weight maps and using pixel-based dark channel prior, respectively. Hence, as indicated in the foreground images of Figures 4–9, the values acquired by the PSNR metric for the compared methods are obviously lower than those attained for the proposed method. Additionally, the values acquired by the MD metric are also higher for the proposed method. As such, the evaluation results demonstrate that the foreground structures are excessively restored by the use of these traditional state-of-the-art methods.

According to this sophisticated quantitative comparison, the proposed method attains the best efficacy of all compared methods, which means that the proposed method is capable of superior visibility restoration in hazy scenarios.

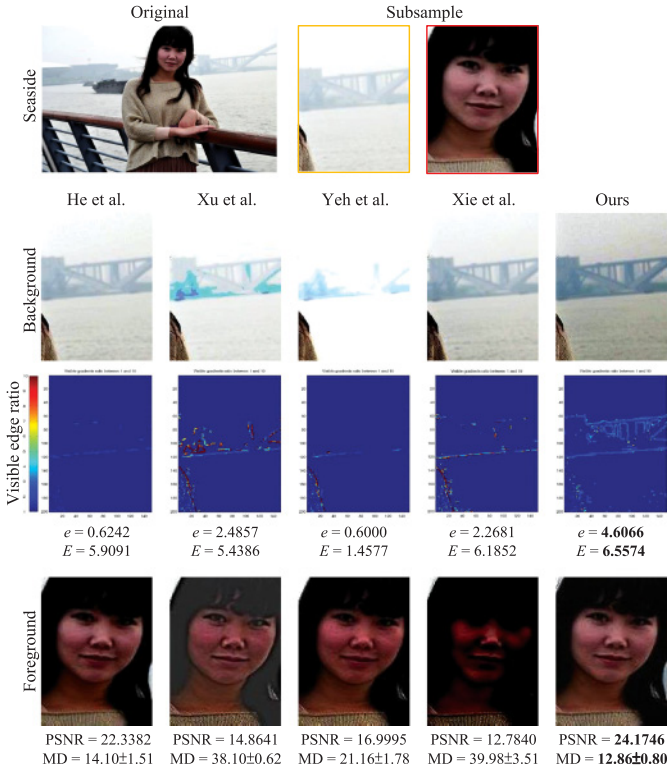

Fig. 4. Restoration efficacy comparison of four different haze removal methods applied to the "Seaside" image, accompanied by two types of subimage rank.

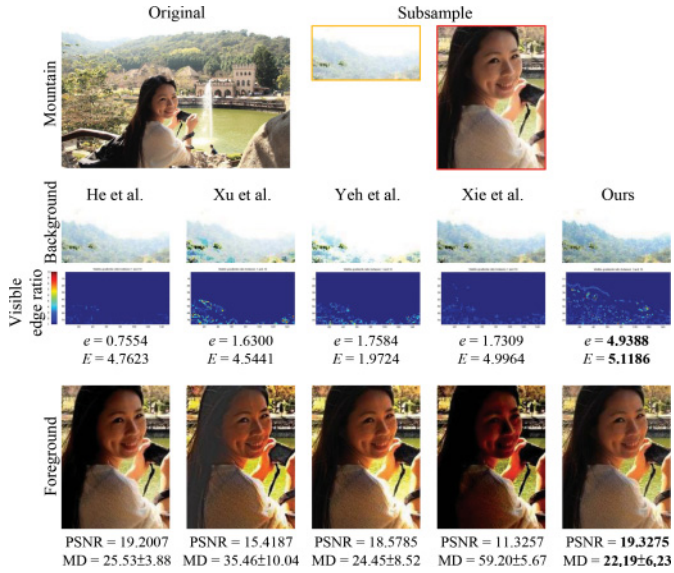

Fig. 5. Restoration efficacy comparison of four different haze removal methods applied to the "Mountain" image, accompanied by two kinds of subimage rank.

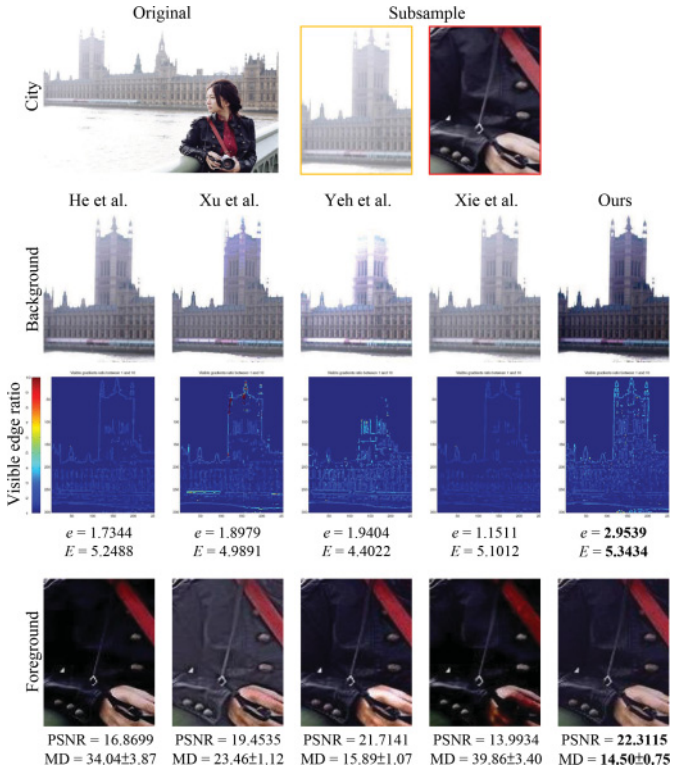

Fig. 6. Restoration efficacy comparison of four different haze removal methods applied to the "City" image, accompanied by two kinds of subimage rank.

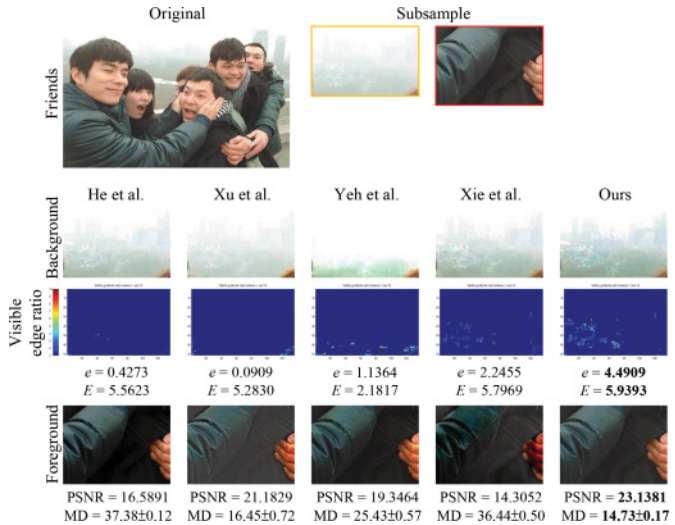

Fig. 7. Restoration efficacy comparison of four different haze removal methods applied to the "Friends" image, accompanied by two kinds of subimage rank.

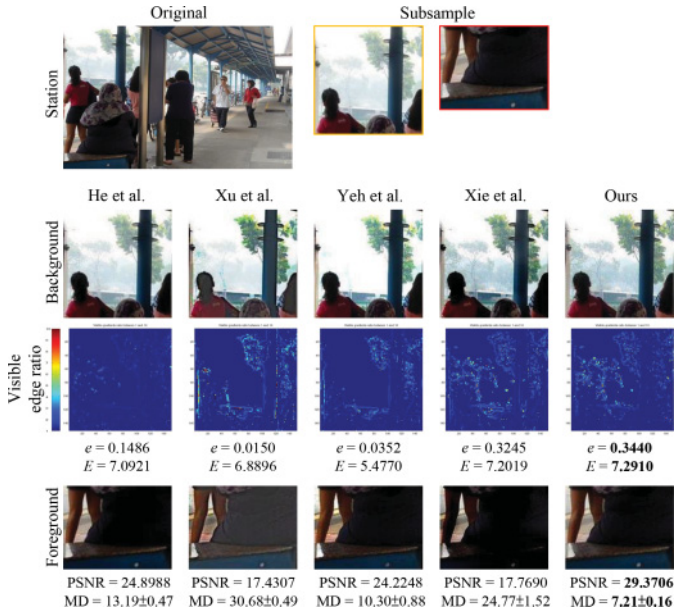

Fig. 8. Restoration efficacy comparison of four different haze removal methods applied to the "Station" image, accompanied by two kinds of subimage rank.

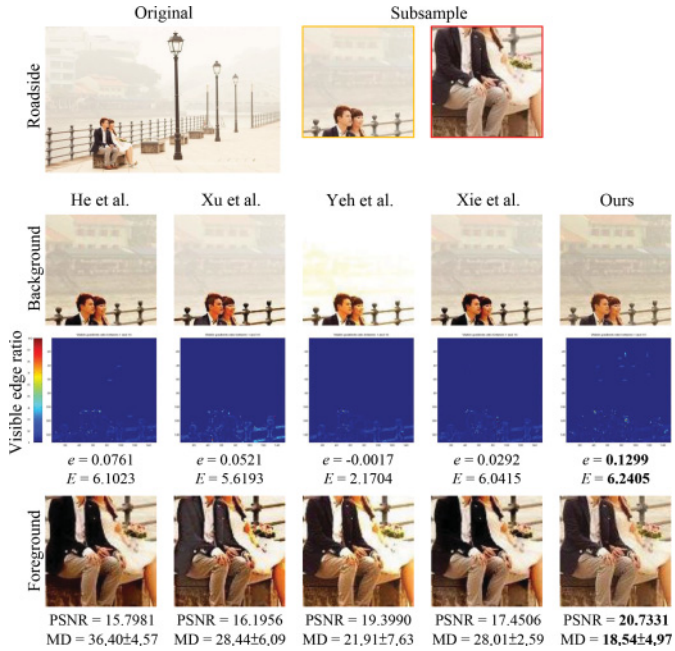

Fig. 9. Restoration efficacy comparison of four different haze removal methods applied to the "Roadside" image, accompanied by two kinds of subimage rank.

Fig. 10. Limitation of the proposed method. (a) and (b) Input hazy images; (c) and (d) their corresponding dark channel with the estimated atmospheric light indicated by circles; (e) and (f) the restored images.

4. CONCLUSIONS

In this article, we presented the limitations of the traditional state-of-the-art haze removal methods by which restored images usually suffer from either the generation of serious artifacts or the loss of object information when captured images of real-world scenes with deep depth of field contain haze only in their background areas. Hence, this article proposed a Bi-Histogram modification-based haze removal method by which to completely and accurately achieve visibility restoration for images captured in hazy weather conditions. To this end, the proposed method uses two major modules. The proposed HDE module first constructs a complete and accurate estimation of haze density via Bi-Histogram modification for overcoming the problems caused by the use of an unbalanced transmission map. Next, the proposed HFR module is able to use the haze density estimation to remove haze formation and avoid generation of artifacts within both background and foreground regions. Consequently, a high-quality, haze-free image with clear visibility can be produced by using the proposed method. According to both qualitative and quantitative evaluations conducted via the use of natural hazy images and detailed in the Experimental Results section of our article, our results demonstrate that the proposed method achieves superior restoration efficacy in comparison with the other state-of-the-art approaches.

In addition, since the proposed method is based on the optical model of Equation (1), it may not be appropriate for some particular images. This is especially true when the constant-airlight assumption of this model is physically invalid. Two examples are shown in Figures 10(a) and 10(b). Estimation of atmospheric light by using the proposed method suffers from both sunlight and headlights, as indicated in Figures 10(c) and 10(d). This results in the estimated atmospheric light being brighter than the real atmospheric light in the other regions. In this case, the restored images look darker than they should be, as shown in Figures 10(e) and 10(f). Because of the problematic nature of this issue, we included an investigation into it in our previous article [Huang et al. 2014].

REFERENCES

L. Caraffa and J.-P. Tarel. 2013. Markov random field model for single image defogging. In *IEEE Intelligent Vehicles Symposium (IV)*. 994–999. DOI:http://dx.doi.org/10.1109/IVS.2013.6629596

J. Y. Chiang and Y.-C. Chen. 2012. Underwater image enhancement by wavelength compensation and dehazing. *IEEE Transactions on Image Processing* 21, 4 (April 2012), 1756–1769. DOI:http://dx.doi.org/10.1109/TIP.2011.2179666

R. Fattal. 2008. Single image dehazing. *ACM Transactions on Graphics* 27, 3, Article 72 (Aug. 2008), 9 pages. DOI:http://dx.doi.org/10.1145/1360612.1360671

N. Hautière, J.-P. Tarel, D. Aubert, and È. Dumont. 2011. Blind contrast enhancement assessment by gradient ratioing at visible edges. *Image Analysis & Stereology* 27, 2, 87–95. DOI:http://dx.doi.org/10.5566/ias.v27.p87-95

K. He, J. Sun, and X. Tang. 2011. Single image haze removal using dark channel prior. *IEEE Transactions on Pattern Analysis and Machine Intelligence* 33, 12 (Dec 2011), 2341–2353. DOI:http://dx.doi.org/10.1109/TPAMI.2010.168

S.-C. Huang and B.-H. Chen. 2014. Automatic moving object extraction through a real-world variable-bandwidth network for traffic monitoring systems. *IEEE Transactions on Industrial Electronics* 61, 4 (April 2014), 2099–2112. DOI:http://dx.doi.org/10.1109/TIE.2013.2262764

S.-C. Huang, B.-H. Chen, and Y.-J. Cheng. 2014. An efficient visibility enhancement algorithm for road scenes captured by intelligent transportation systems. *IEEE Transactions on Intelligent Transportation Systems* 15, 5 (Oct 2014), 2321–2332. DOI:http://dx.doi.org/10.1109/TITS.2014.2314696

S.-C. Huang, F.-C. Cheng, and Y.-S. Chiu. 2013. Efficient contrast enhancement using adaptive gamma correction with weighting distribution. *IEEE Transactions on Image Processing* 22, 3 (March 2013), 1032–1041. DOI:http://dx.doi.org/10.1109/TIP.2012.2226047

J. Kopf, B. Neubert, B. Chen, M. Cohen, D. Cohen-Or, O. Deussen, M. Uyttendaele, and D. Lischinski. 2008. Deep photo: Model-based photograph enhancement and viewing. *ACM Transactions on Graphics* 27, 5, Article 116 (Dec. 2008), 10 pages. DOI:http://dx.doi.org/10.1145/1409060.1409069

A. Levin, D. Lischinski, and Y. Weiss. 2008. A closed-form solution to natural image matting. *IEEE Transactions on Pattern Analysis and Machine Intelligence* 30, 2 (Feb. 2008), 228–242. DOI:http://dx.doi.org/10.1109/TPAMI.2007.1177

X. Li, W. Hu, C. Shen, Z. Zhang, A. Dick, and A. Van Den Hengel. 2013. A survey of appearance models in visual object tracking. *ACM Transactions on Intelligent Systtems and Technology* 4, 4, Article 58 (Oct. 2013), 48 pages. DOI:http://dx.doi.org/10.1145/2508037.2508039

H. Ma, C. Zeng, and C. X. Ling. 2012. A reliable people counting system via multiple cameras. *ACM Transactions on Intelligent Systems and Technology* 3, 2, Article 31 (Feb. 2012), 22 pages. DOI:http://dx.doi.org/10.1145/2089094.2089107

S. G. Narasimhan and S. K. Nayar. 2003a. Contrast restoration of weather degraded images. *IEEE Transactions on Pattern Analysis and Machine Intelligence* 25, 6 (June 2003), 713–724. DOI:http://dx.doi.org/10.1109/TPAMI.2003.1201821

S. G. Narasimhan and S. K. Nayar. 2003b. Interactive (de)weathering of an image using physical models. In *ICCV Workshop on Color and Photometric Methods in Computer Vision (CPMCV)*.

S. K. Nayar and S. G. Narasimhan. 1999. Vision in bad weather. In *The Proceedings of the Seventh IEEE International Conference on Computer Vision*, Vol. 2. 820–827. DOI:http://dx.doi.org/10.1109/ICCV.1999.790306

K. Nishino, L. Kratz, and S. Lombardi. 2012. Bayesian defogging. *International Journal of Computer Vision* 98, 3, 263–278. DOI:http://dx.doi.org/10.1007/s11263-011-0508-1

J. P. Oakley and B. L. Satherley. 1998. Improving image quality in poor visibility conditions using a physical model for contrast degradation. *IEEE Transactions on Image Processing* 7, 2 (Feb. 1998), 167–179. DOI:http://dx.doi.org/10.1109/83.660994

Yoav Y. Schechner, Srinivasa G. Narasimhan, and Shree K. Nayar. 2003. Polarization-based vision through haze. *Applied Optics* 42, 3 (Jan. 2003), 511–525. DOI:http://dx.doi.org/10.1364/AO.42.000511

Y.-H. Shiau, H.-Y. Yang, P.-Y. Chen, and Y.-Z. Chuang. 2013. Hardware implementation of a fast and efficient haze removal method. *IEEE Transactions on Circuits and Systems for Video Technology* 23, 8 (Aug. 2013), 1369–1374. DOI:http://dx.doi.org/10.1109/TCSVT.2013.2243650

X. Song, X. Shao, Q. Zhang, R. Shibasaki, H. Zhao, J. Cui, and H. Zha. 2013. A fully online and unsupervised system for large and high-density area surveillance: Tracking, semantic scene learning and abnormality detection. *ACM Transactions on Intelligent Systems and Technology* 4, 2, Article 35 (April 2013), 21 pages. DOI:http://dx.doi.org/10.1145/2438653.2438670

K. Tan and J. P. Oakley. 2000. Enhancement of color images in poor visibility conditions. In *Proceedings of the IEEE International Conference on Image Processing*, Vol. 2. 788–791. DOI:http://dx.doi.org/10.1109/ICIP.2000.899827

R. T. Tan. 2008. Visibility in bad weather from a single image. In *IEEE Conference on Computer Vision and Pattern Recognition*. 1–8. DOI:http://dx.doi.org/10.1109/CVPR.2008.4587643

J.-P. Tarel and N. Hautiere. 2009. Fast visibility restoration from a single color or gray level image. In *IEEE 12th International Conference on Computer Vision*. 2201–2208. DOI:http://dx.doi.org/10.1109/ICCV.2009.5459251

B. Xie, F. Guo, and Z. Cai. 2010. Improved single image dehazing using dark channel prior and multi-scale retinex. In *International Conference on Intelligent System Design and Engineering Application (ISDEA)*, Vol. 1. 848–851. DOI:http://dx.doi.org/10.1109/ISDEA.2010.141

H. Xu, J. Guo, Q. Liu, and L. Ye. 2012. Fast image dehazing using improved dark channel prior. In *International Conference on Information Science and Technology (ICIST)*. 663–667. DOI:http://dx.doi.org/10.1109/ICIST.2012.6221729

C.-H. Yeh, L.-W. Kang, M.-S. Lee, and C.-Y. Lin. 2013. Haze effect removal from image via haze density estimation in optical model. *Optics Express* 21, 22 (Nov. 2013), 27127–27141. DOI:http://dx.doi.org/10.1364/OE.21.027127

S. Zhang, H. Yao, X. Sun, and S. Liu. 2012. Robust visual tracking using an effective appearance model based on sparse coding. *ACM Transactions on Intelligent Systems and Technology* 3, 3, Article 43 (May 2012), 18 pages. DOI:http://dx.doi.org/10.1145/2168752.2168757

Received August 2014; revised December 2014; accepted December 2014